Using Nitrogen Isotope Fractionation to Assess the Oxidation of Substituted Anilines by Manganese Oxide

Journal:	*Environmental Science & Technology*
Manuscript ID:	es-2011-00743t.R1
Manuscript Type:	Article
Date Submitted by the Author:	02-May-2011

Complete List of Authors:	Skarpeli-Liati, Marita; Eawag, Environmental Chemistry Jiskra, Martin; ETH Zürich, Institute for Biogeochemistry and Pollutant Dynamics Garr, Asley; University of Minnesota, Chemistry Turgeon, Aurora; University of Minnesota, Chemistry Arnold, William A.; University of Minnesota, Department of Civil Engineering Cramer, Christopher; University of Minnesota, Chemistry Schwarzenbach, René; ETH Zürich, Institute for Biogeochemistry and Pollutant Dynamics Hofstetter, Thomas; Eawag, Environmental Chemistry

Using Nitrogen Isotope Fractionation to Assess the Oxidation of Substituted Anilines by Manganese Oxide

Marita Skarpeli-Liati,[†] Martin Jiskra,[‡] Aurora Turgeon,[¶] Ashley N. Garr,[¶] William A. Arnold,[§] Christopher J. Cramer,[¶] René P. Schwarzenbach,[‡] and Thomas B. Hofstetter[*,†]

Eawag, Swiss Federal Institute of Aquatic Science and Technology, CH-8600 Dübendorf, Switzerland, Institute of Biogeochemistry and Pollutant Dynamics (IBP), ETH Zürich, CH-8092 Zürich, Switzerland, Department of Chemistry and Supercomputing Institute, University of Minnesota, Minneapolis, MN 55455, and Department of Civil Engineering University of Minnesota, Minneapolis, MN 55455

E-mail: thomas.hofstetter@eawag.ch

[*]To whom correspondence should be addressed
[†]Eawag and ETH Zürich
[‡]ETH Zürich
[¶]Department of Chemistry and Supercomputing Institute, University of Minnesota
[§]Department of Civil Engineering, University of Minnesota

Abstract

We explored the N isotope fractionation associated with the oxidation of substituted primary aromatic amines, which are often the position of initial attack in transformation processes of environmental contaminants. Apparent ^{15}N-kinetic isotope effects, $AKIE_N$, were determined for oxidation of various substituted anilines in suspension of manganese oxide (MnO_2) and compared to reference experiments in homogeneous solution and at electrode surfaces, as well as to density functional theory calculations of intrinsic KIE_N for electron and hydrogen atom transfer reactions. Owing to the partial aromatic imine formation after one-electron oxidation and corresponding increase in C–N bond strength, $AKIE_N$-values were *inverse*, substituent-dependent, and confined to the range between 0.992 and 0.999 in agreement with theory. However, $AKIE_N$-values became *normal* once the fraction of cationic species prevailed owing to ^{15}N-equilibrium isotope effects, EIE_N, of 1.02 associated with N atom deprotonation. The observable $AKIE_N$-values are substantially modulated by the acid/base pre-equilibria of the substituted anilines and isotope fractionation may even vanish under conditions where normal EIE_N and inverse $AKIE_N$ cancel each other out. The pH-dependent trends of $AKIE_N$-values provide a new line of evidence for the identification of contaminant degradation processes via oxidations of primary aromatic amino groups.

Introduction

Aromatic amino groups are often the position of initial attack in transformation processes of industrial chemicals, biocides, and pharmaceuticals in the environment (*1–6*). A (quantitative) assessment of these processes is therefore essential for evaluating the exposure and impact of these micropollutants on human and environmental health (*7*). However, aryl amines can react along different, sometimes competing pathways including the mineral- and enzyme-catalyzed oxidation of the N atom (*1–3*), the microbial dioxygenation of the aromatic ring (*8*), as well as through nucleophilic addition of the amino functional group to electrophilic sites of natural organic matter (*9*). Identifying these transformation processes is also challenging because they give rise to products that are usually difficult to analyze quantitatively (e.g., radical coupling products, adducts to NOM etc.).

Compound specific isotope analysis (CSIA) has been shown to offer new avenues to track degradation processes of such N-containing contaminants, even if competing reaction pathways occur and reaction products are partially unknown (*10–12*). This is because stable isotope compositions measured in the remaining fraction of the contaminant molecule over time or distance from the pollution source change systematically depending on the type of chemical bond(s) that are broken or formed as a consequence of kinetic or equilibrium isotope effects (*13*). As shown for nitroaromatic explosives (*14–16*), phenylurea (*17*, *18*) and triazine herbicides (*19–21*), their enzymatic, abiotic, and photochemical redox reactions lead to typical distinct trends of C, H, and N isotope signatures that are not only indicative for the active transformation processes but can also allow one to quantify the extent of their degradation. These observations are due to the fact that different (N-containing) functional groups are involved in reactions, which also exhibit distinct apparent ^{13}C-, ^{2}H-, and ^{15}N-kinetic isotope effects (AKIEs). Despite the importance of aromatic amine oxidation for contaminant transformations, their isotope effects are largely unknown.

The goal of the present study was to assess the isotope effects associated with the oxidation of aromatic amino groups under typical environmental conditions and to evaluate whether the isotope fractionation associated with contaminant transformation can be exploited by CSIA for

tracking these processes in aquatic environments. As a first step, we investigated the magnitude and variability of apparent ^{15}N-kinetic isotope effects ($AKIE_N$) during the abiotic oxidation of a series of substituted anilines in suspensions of manganese oxide (MnO_2), which represents an important heterogenous oxidant in the environment. Oxidation of substituted anilines by MnO_2 was reported to proceed via initial electron transfer from the lone pair of the nitrogen leading to formation of arylamino radicals (*1*, *2*). As shown recently for the reduction of nitroaromatic radical anions (*14*, *22*), even such small bonding changes induced by electron transfer to and from N atoms are likely to generate N isotope fractionation than can be measured by ^{15}N-CSIA.

Here, we examine the N isotope fractionation of a series of *o*-, *m*- and *p*-substituted anilines covering more than one order of relative reactivities (*1*). Product analysis was performed to corroborate the proposed initial reaction mechanism involving substituted aniline radicals. Because the investigated compounds exhibit pK_{BH^+}-values between 4.0 and 5.3, we examined potential effects of contaminant speciation and contributions of ^{15}N-equilibrium isotope effects due to aromatic amine deprotonation (*23*) to the observable $AKIE_N$ through experiments conducted in MnO_2 suspension at pH-values between 4.0 and 7.0. Finally, independent evidence for the interpretation of N isotope fractionation was obtained (i) from homogeneous and electrochemical oxidation experiments and (ii) from computations of ^{15}N-kinetic isotope effects (KIE_N) pertinent to outer-sphere electron transfer and H atom transfer from substituted anilines using density functional theory.

Experimental Section

A complete list of all used chemicals including purities and suppliers, as well as a detailed description of the preparation and characterization procedures of MnO_2-suspension can be found in the Supporting Information (SI).

Experimental systems for the oxidation of substituted anilines

MnO_2-suspensions

MnO_2 particles were synthesized through oxidation of Mn^{2+} by MnO_4^- according to the method of Murray (*24*). The suspensions were prepared in 10 mM acetate buffer for experiments carried out at pH 4.0 and 5.1 and in 10 mM phosphate buffer for experiments at pH 7.0. XRD-measurements indicated that the synthesized MnO_2-mineral was highly amorphous with Mn oxidation state 3.9$\pm$0.3 as determined by iodometric titration and the pH_{IEP} was 3.25$\pm$0.09 as obtained from ζ-potential measurements (see SI).

Oxidation of substituted anilines by MnO_2 was carried out in batch reactors containing different concentrations of MnO_2 in buffer solutions, NaCl (final ionic strength to 0.02 M), and a PTFE-coated magnetic stirring bar. All batch experiments were conducted at room temperature under oxic conditions. Losses of the reactants due to volatilization, oxidation by air and/or sorption to the Viton rubber stoppers were accounted for in reference experiments set up in the identical manner except for the addition of MnO_2. Note that lack of reactivity of some substituted anilines in MnO_2-suspensions as well as in reference experiments (oxidation by $ABTS^{\bullet-}$ (2,2'-azino-bis(3-ethylbenzthiazoline-6-sulfonic acid) radical anion) in aqueous solution and at electrode surfaces) limited the selection of substituted anilines (SI, Chapter 2).

Experiments at pH 7.0 were conducted in duplicates. The reaction was initiated by the addition of variable amounts of substituted anilines from a methanolic stock solution to achieve initial concentrations of 400-600 μM. The MnO_2 concentrations were varied so that fast reactions did not exceed 50% conversion within the first minute of the experiment, while the oxidative turnover of slowly reacting compounds had to be >60% within 3 days. Samples were withdrawn at pre-defined time points with a gas tight glass syringe and the oxidation reaction was stopped by filtering off MnO_2-particles with a 0.2 μm regenerated cellulose (RC) filter. Filtered solutions were stored in amber vials in the dark at 4°C until concentration measurements and isotope analysis. Because the disappearance of substituted anilines from MnO_2-suspensions at pH 4.0 and 5.1 was too fast to be

sampled as described for pH 7.0, variable amounts of MnO_2 were spiked to reactors containing the identical initial concentration of substituted aniline. This procedure was used to achieve different degrees of reactant conversion and was shown earlier for nitroaromatic compounds to enable the study of isotope fractionation of fast reactions (*14*). Prior to concentration measurements and isotope analysis of substituted anilines, the pH of the filtered aqueous samples was adjusted to pH 7.0 with NaOH.

The loss of substrate due to adsorption and cation exchange to the mineral surface was assessed for aniline by experiments in which the compound's concentration was compared before and after reductive dissolution of the MnO_2-particles with ascorbic acid (0.3 M, pH 13) at different time points of the reaction. To this end, the aniline was extracted from the aqueous solution with ethyl acetate and the concentration in the extract was quantified by GC/MS. The extraction efficiency of aniline into ethyl acetate was 99.5±2.5%.

For the identification of organic oxidation products by LC-MS/MS, samples of 1 mL MnO_2-suspension were reductively dissolved by ascorbic acid (0.3 M, pH 13) and diluted with 9 mL of nanopure water. Aqueous samples were processed following a modified procedure of (*25*). Inorganic salts were removed by solid phase extraction (SPE, HLB Extraction Cartridges, 100 μm, Oasis, Waters AG, U.S.) of the dilute aqueous samples. Organic analytes were eluted from the cartridges with MeOH, dissolved in H_2O and filtered with a 0.45 μm RC filter prior to LC-MS/MS.

Homogeneous oxidation

Oxidation of substituted anilines in homogeneous solution was performed in an anoxic glovebox using anoxic stock and buffer solutions identical to experiments with MnO_2-suspensions at pH 4.0 and 5.1 (see above), except for the addition of variable amounts of electrochemically produced oxidant instead of MnO_2 to achieve different degrees of contaminant conversion. The oxidant $ABTS^{\bullet -}$ was generated through direct electrochemical oxidation of the $ABTS^{2-}$ at an E_h of 0.667 V (SHE) in the electrochemical cell as described in (*26*). The ABTS dianion was added to buffer

solutions (0.1 M phosphate at pH 7.0 and 0.1 M acetate at pH 4.0 in 0.1 M KCl as supporting electrolyte) and the oxidative working current was monitored until it dropped below background values (30 μA). The $ABTS^{\bullet-}$ was used immediately after generation. All samples containing the residual substituted aniline were stored at 4°C until concentration and isotope ratio analysis.

Direct electrochemical oxidation

All electrochemical experiments were conducted in an anoxic glovebox using anoxic stock and buffer solutions (0.1 M acetate and phosphate for pH 4.0 and 7.0, respectively) containing 0.1 M KCl as background electrolyte (see (*26*) for procedures). Direct electrochemical oxidation of the aromatic amines was performed in an electrolysis cell equipped with a glassy carbon (GC) working electrode, an Ag/AgCl reference electrode, and a coiled platinum wire auxiliary electrode as described in (*26*). Currents were measured with an CHInstruments 630C instrument (Austin, TX, USA) and the potential was controlled by an Autolab PG 302 instrument (EcoChemieB.V., Utrecht, NL). The electrolysis cell was filled with the corresponding buffer solution and equilibrated at the desired reduction potential (E_h between 0.777 and 0.957 V vs. SHE, Table 1) applied to the working electrode. The oxidation was initiated by the addition of defined amounts of substituted aniline stock solution. At given time intervals, 2 mL aqueous samples were withdrawn and stored outside the glovebox at 4°C until further analysis.

Analytical Methods

Chemical analysis

Concentration measurements of substituted anilines were performed by reversed-phase HPLC (Supelcosil LC-18, 25 cm $\times$ 4.6 mm, 5μm, Supelco) and UV-VIS detection at wavelengths corresponding to the absorption maxima of the anilines. Different eluent mixtures KH_2PO_4/MeOH were used for each compound varying between 40/60% to 70/30% at a flow rate of 1 mL min^{-1} and sample injection volume of 10 μL. Quantification of substituted anilines extracted into ethyl

acetate was conducted on a GC/MS (Ultra Trace GC and DSQII, Thermo Electron Corporation) upon on-column injection using the instrumental setup and settings described previously (*23*).

The analytical procedure for identification of transformation products was adapted from (*25*). The measurements were performed by liquid chromatography coupled to an LTQ (Linear Trap Quadrupole) Orbitrap mass spectrometer (Thermo Electron Corporation) with electrospray ionization (LC-MS/MS). For liquid chromatographic separation a XBridge C-18 column was used (2.1 $\times$ 50 mm, 3.5 μm particle size, Waters) and a gradient was run from H_2O/MeOH 90/10% to 5/95% containing 0.1% formic acid. Identification of coupling products was performed only qualitatively due to lack of commercial standards. To this end exact masses of expected reaction products were extracted from the chromatograms in order to obtain MS/MS-fragment spectra. Based on the exact molecular mass and fragmentation pattern of each detected product, most probable molecular structures were postulated and these are shown in Figure S1.

The aqueous Mn^{2+}-concentration was measured by inductively coupled plasma mass spectrometry (ICP/MS 7500cx, Agilent Technologies). All samples were diluted with 0.1 M HNO_3 to final concentrations between 10 and 1000 μg Mn^{2+} L^{-1}.

Stable isotope ratio measurements

Stable N and C isotope signatures (δ^{15}N and δ^{13}C) of the substituted anilines were determined by solid-phase microextraction (SPME) coupled to a GC/IRMS (gas chromatography isotope-ratio mass spectrometry) with combustion interface (*23*). SPME fiber material and extraction conditions were polydimethylsiloxane/divinylbenzene (PDMS/DVB, Supelco) and 45 min at 40°C for all compounds except OCH_3-substituted anilines. The latter required DVB-Carboxen-PDMS coated fibers and 45 min extractions at 70°C. All N and C isotope signatures are reported as arithmetic mean ($\pm 1\sigma$) of triplicate measurements relative to air ($\delta^{15}N_{air}$) and Vienna PeeDee Belemnite ($\delta^{13}C_{VPDB}$), respectively, in per mil (‰). To account for uncertainty due to instrument nonlinearity (*27*) all samples were diluted to concentrations yielding constant peak amplitudes (1-2 V for ^{15}N- and 4-5 V for ^{13}C-analysis). Accuracy of compound-specific isotope analysis was verified

via standard bracketing procedures using a calibrated in-house standard (aniline) of known N and C isotope ratios (*23*).

Data Evaluation

Bulk compound N and C isotope enrichment factors, ε_N and ε_C, were derived from linear regression analysis of δ^{15}N- and δ^{13}C-values, respectively, vs. fractional amount of reactant conversion (*10*). Data from replicate experiments were combined using the Pitman estimator (*28*) as shown previously (*29*). While the extent of C isotope fractionation is reported as average ε_C for all C atoms present in the reactant molecules, interpretation of N isotope fractionation is based on position-specific apparent ^{15}N-kinetic isotope effects, AKIE$_N$, calculated from Eq. (1). Uncertainties associated with ε_N-, ε_C-, AKIE$_N$-values correspond to 95% confidence intervals.

$$\text{AKIE}_N = \frac{1}{1+\varepsilon_N/1000} \tag{1}$$

To account for effects of substituted aniline protonation on the observed AKIE$_N$s, data obtained at pH-values below 7.0 were modeled as follows (see SI for full mathematical derivation). N isotope fractionation of substituted aniline cations, BH^+, originates from the combination of an isotope-sensitive deprotonation step (Eq. (2), (*23*)) and the subsequent oxidation reaction of the neutral species, B (Eq. (3)).

$$BH^+ \underset{k_2}{\overset{k_1}{\rightleftharpoons}} B + H^+ \tag{2}$$

$$B \xrightarrow{k_3} P \tag{3}$$

where k_1, k_2 and k_3 are the reaction rate constants of the elementary reactions and P stands for the radical products of the oxidation reaction. Using the steady-state treatment for the proton-exchange pre-equilibrium, the rate constant for the reaction of protonated substituted aniline species $k_{obs}^{BH^+}$ is

given by Eq. (4).

$$k_{obs}^{BH^+} = \frac{k_1 \times k_3}{k_2[H^+] + k_3} \quad (4)$$

where $[H^+]$ is the proton concentration. Rewriting Eq. (4) for ^{14}N- and ^{15}N-isotopologues (see SI) reveals that an apparent ^{15}N-kinetic isotope effect associated with species BH^+, $AKIE_N^{BH^+}$, is the product of the deprotonation ^{15}N-equilibrium isotope effect, $EIE_N^{BH^+}$, and the $AKIE_N$ of the neutral substituted aniline, $AKIE_N^B$ (Eq. (5)).

$$AKIE_N^{BH^+} = EIE_N^{BH^+} \times AKIE_N^B \quad (5)$$

As a consequence of the simultaneous reactions of protonated and neutral substituted aniline species, the overall observable $AKIE_N$ is the weighted average of the two fractions and their respective isotope effect. In Eq. (6), f_{BH^+} is the fraction of protonated compound, which equals $\left(1 + 10^{(pH - pK_{BH^+})}\right)^{-1}$ (see Table S3 for pK_{BH^+}).

$$AKIE_N = f_{BH^+} \times EIE_N^{BH^+} \times AKIE_N^B + \left(1 - f_{BH^+}\right) \times AKIE_N^B \quad (6)$$

Computational Methods

The gas-phase geometries of all molecular species were fully optimized at the density functional (DFT) level using the gradient-corrected Perdew-Wang exchange and correlation functionals (*30*, *31*) as modified by Adamo and Barone (*32*) using either the 6-311+G(d) or 6-311+G(2df,2p) basis sets (*33*). Stationary points were confirmed as minima or transition-state (TS) structures by analytical calculation of vibrational frequencies, which were also used in the construction of ideal-gas, rigid-rotator, harmonic oscillator partition functions, from which thermal contributions to free energies G were computed (*34*). For outer-sphere electron-transfer rate constants, ^{15}N-kinetic isotope effects (KIE_Ns) were computed essentially according to the method of Kavner et al. (*35*). For hydrogen-atom transfer reactions involving active oxygen species, KIEs were computed from

canonical transition-state theory. Full details of all KIE_N calculations are provided in the SI.

Results and discussion

Isotope fractionation associated with the oxidation of substituted anilines in MnO_2-suspensions.

We observed measurable N isotope fractionation during the oxidation of neutral, substituted anilines in suspensions of MnO_2 at pH 7.0, while C isotope composition did not change significantly. Nitrogen isotope fractionation was always *inverse*, that is, ^{15}N-containing isotopologues reacted faster than molecules with ^{14}N leading to a decreasing $\delta^{15}N$ of the reactant with increasing conversion (Figure 1b). The extent of N isotope fractionation observed in suspensions of MnO_2 did not exceed –12‰ compared to the initial $\delta^{15}N$ while the reactant turnover approached 55 to 88% (Table 1). Limited turnover was due to the biphasic disappearance kinetics of substituted aniline oxidation by MnO_2 (Figure 1a), which, as reported previously (*1*, *2*, *36*), exhibited fast initial transformation followed by a decreasing rate of reaction. Increasing the concentration ratio of MnO_2 to substituted aniline slightly increased the oxidative turnover and thus the observable range of N isotope fractionation (Figure 1b) but did not influence the N isotope enrichment factors, ε_N, which quantify the extent of isotope fractionation per incremental amount of reacted substrate (Figure 1b and 1c). As shown in Figure 1c, ε_N-values of aniline oxidation were identical within experimental error. This observation suggests that despite biphasic reaction kinetics, N isotope fractionation was associated with the identical elementary reaction step(s) of aromatic amine oxidation independent of the substituted aniline to oxidant ratio.

The occurrence of a single isotope fractionating elementary reaction step was confirmed with a series of complementary experiments, which showed that the biphasic reaction kinetics were due to a decrease in MnO_2 reactivity rather than a change in substituted aniline oxidation mechanism during the time course of the reaction. First, the decreasing rate of contaminant disappearance correlated with the decreasing average particulate Mn oxidation state monitored by X-ray absorp-

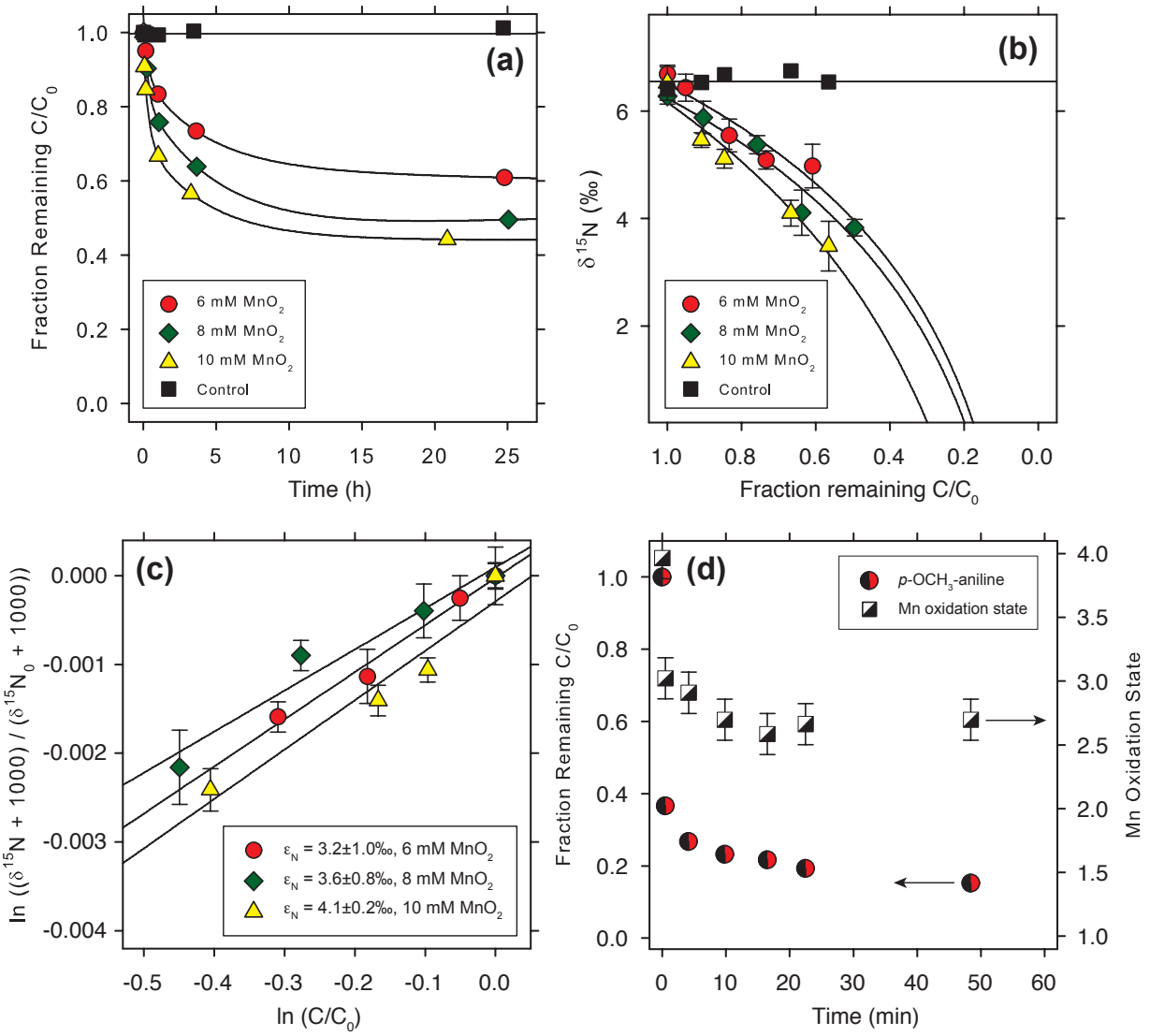

Figure 1: (a) Kinetics of unsubstituted aniline oxidation (C_0 = 0.6 mM) in suspensions containing 6, 8, and 10 mM MnO_2 at pH 7.0. Uncertainty of the concentration measurements ($\pm\sigma$) is 2% (error bars are smaller than the markers); (b) N isotope fractionation during aniline oxidation in various MnO_2-suspensions: δ^{15}N-values vs. fraction of remaining reactant (C/C_0); (c) linearized N isotope fractionation trends used for calculation of bulk N isotope erichment factors: ε_N; (d) Oxidation of *p*-OCH_3-aniline (4.8 mM initial concentration) in 10 mM MnO_2suspension at pH 7.0 and average Mn oxidation state.

tion near edge structure (XANES) measurements, as illustrated in Figure 1d for the oxidation of *p*-OCH_3-aniline by MnO_2. The average Mn oxidation state decreased to 2.6 during the time course of the reaction pointing to an increased share of reduced Mn species in the mineral including Mn(II) adsorbed on the mineral surface. The corresponding decrease of average Mn oxidation

state is indicative of the decreasing reactivity of the MnO_2-particles. The same process has been invoked previously for the reductive dissolution of MnO_2 (e.g., by arsenious acid, H_3AsO_3), where formation of intermediate Mn(III)oxyhydroxide layers at the mineral surface blocked the access to reactive oxidized Mn(IV) sites and led to the overall decrease of the MnO_2 reduction rate (*37*, *38*). Measurements of dissolved Mn^{2+} at different time points of unsubstituted aniline oxidation by MnO_2 support the interpretation of XANES-data (Figure S3). After a conversion of > 400 μM of the initial 600 μM of aniline, only 130 μM of Mn^{2+}_{aq} were recovered in solution. Therefore, only 65% of the oxidation equivalents of aniline could be detected as dissolved species, leaving Mn^{3+}- and Mn^{2+}-species bound to the mineral. Second, identical aniline disappearance kinetics were observed regardless whether aniline was measured in the supernatant or after dissolving the MnO_2-particles (Figures S3). Similarly, no inhibition of the reaction was found if Mn^{2+} and azobenzene had been added to the reactors in concentrations corresponding to the initial aniline oxidation-equivalents (Figures S4). These experiments indicate that under the experimental conditions, neither adsorption of aniline nor of co-solutes to MnO_2 did influence the rate of aniline oxidation (*1*, *2*). Finally, identical ε_N-values for different MnO_2-loadings provide evidence that an electron transfer process is rate-limiting rather than any surface complex formation between the substituted aniline and the mineral. The assumption of an electron transfer as predominant rate-limiting step is also supported by the reported correlation of the half-wave potentials and substituent Hammett constants of the aromatic amines with experimentally determined initial oxidation rates (*1*, *2*).

Substituent effects on $AKIE_N$s and implications for the reaction mechanism

Based on the above discussion, the observable N isotope fractionation with ε_N-values between 1.3‰ and 8.3‰ can be attributed to the oxidation of the N atom in neutral substituted anilines resulting in apparent ^{15}N-kinetic isotope effects, $AKIE_N$ between 0.9987 and 0.9927 (Table 1, entries no. 1-8). The small C isotope fractionation represents an average secondary isotope effect for the C atoms that were not directly involved in the reaction (ε_C of -1.1 ± 0.1‰, Figure S2).

We observed a marked influence of the position and type of the aromatic substituent on $AKIE_N$-values. *Meta*-substitution with -CH_3 or -OCH_3-groups did not cause the $AKIE_N$-value to deviate significantly from that of aniline (0.9960±0.0009). Electron-donating substituents in *ortho* or *para* position, however, led to larger N isotope fractionation (lowest $AKIE_N$ of 0.9927±0.0012 for *p*-OCH_3-aniline, entry 7, Table 1) compared to unsubstituted aniline, while electron-accepting substituents caused the opposite trend ($AKIE_N$ of 0.9987±0.0004 for *p*-Cl-aniline, entry 8, Table 1). The identical $AKIE_N$-values within experimental error found for *o*-CH_3 and *p*-CH_3-aniline as well as *o*-OCH_3 and *p*-OCH_3-aniline, respectively, indicate that substituents in these positions exhibited the same effects on the bonds to N during its oxidation.

The observed inverse isotope effects can be rationalized by the formation of a radical intermediate after one-electron oxidation, which is delocalized over the aromatic ring causing the C–N-bond to become stronger in the transition state, due to the formation of a partial imine-type bonding of N in the subsequent intermediates (illustrated by the resonance structures in Scheme 1). Higher infrared stretching frequencies of C=N *vs.* C–N bonds (*39*) imply stronger bonds to N in imines and support this interpretation. Similar findings of inverse N isotope fractionation have been reported for reactions in which additional bonds were formed to aromatic and heterocyclic N atoms and in amino acids (*20*, *23*, *40*, *41*). In addition, the formation of radical intermediates gives rise to the sensitivity of the $AKIE_N$-values for aromatic substitution. The substituents' electron donating and accepting properties affect the radical stability, the preferential radical localization in *ortho*- and *para*-position, and thus the C–N bond strength in the transition state, which explains the observed variations of the $AKIE_N$. While electron donating substituents like *o*-/*p*-CH_3 and *o*-/*p*-OCH_3 cause the C–N-bond to become stronger in the transition state, electron-withdrawing *p*-Cl substitution has only moderate impact on C–N bonding and thus the magnitude of the $AKIE_N$ compared to the unsubstituted aniline. Consequently, the lack of any radical stabilization and thus localization in *meta*-position is also responsible for the insensitivity of the $AKIE_N$ for *meta*-substituents. Analysis of reactor solutions for reaction products by LC-MS/MS confirmed these substituent effects indirectly. As proposed in previous studies (*2*, *3*), head-to-head (N–N), head-to-tail (N–C) and

tail-to-tail (C–C) products were found in the reduced as well as in the oxidized form, where radical coupling occurred at the *ortho* and *para* position.

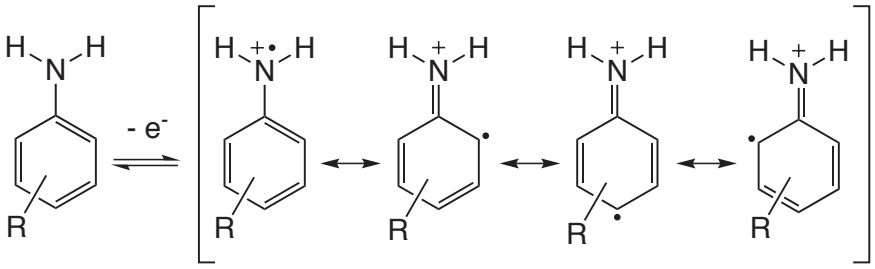

Scheme 1

Reference experiments and density functional theory calculations

Independent evidence for assigning the one-electron oxidation and subsequent partial imine-bond formation as isotope-sensitive and rate-limiting reaction step was obtained from measurements of N isotope fractionation of selected substituted anilines in homogeneous solution, in electrochemical experiments, and through calculation of KIE_N using density functional theory. Despite the different experimental conditions, oxidation of aniline and *p*-CH_3-aniline by $ABTS^{\bullet-}$ and at glassy carbon electrode surfaces at pH 7.0 also resulted in inverse $AKIE_N$s as observed in MnO_2-suspensions (Table 1). $AKIE_N$-values pertinent to electrochemical oxidation of *p*-CH_3-aniline at oxidation potentials differing by 180 mV, which corresponds to three orders of magnitude in electron transfer driving force, did vary by less than 2.5‰ (Figure 2a, Table 1, entries 19-22). The insensitivity of N isotope fractionation towards oxidation potential lends further support to the hypothesis that N isotope fractionation during substituted aniline oxidation is not caused exclusively by the electron transfer but also by hybridization changes at the N atom and change in C–N bond strength during formation of partial imine bonds. This interpretation is also supported by theoretical considerations.

Density functional calculations were undertaken to predict KIE_Ns that would be expected under conditions of outer-sphere electron transfer (ET) and hydrogen-atom transfer (HAT) by an active oxygen species (Table S1). In the former case, isotopically sensitive rate constants were predicted

from Marcus theory; in the latter case, such constants were predicted from canonical transition-state theory (see SI for full theoretical details). Table S1 (entries 25-37) provides the predicted KIE_Ns for aniline and various substituted cases. In general, there is good quantitative agreement between the predicted KIE_Ns for ET and those determined experimentally (at pH 7.0, see electrochemical data below) with electrodes having reduction potentials similar to those employed in the calculations. The HAT-KIE_Ns are also generally in good quantitative agreement with those determined experimentally at pH 7.0. All predicted KIE_Ns are inverse (with the exception of HAT from *o*-NO_2-aniline by hydroxyl radical), reflecting the increased C_1–N bonding in the anilinium radical cation or HAT transition state structure compared to the reactant aniline (Scheme 1, for quantitative comparisons, see computed geometrical and bond order data in Table S2). The quantitative similarity for the two processes is primarily attributable to the small change in this bonding character, which leads to predicted inverse KIE_Ns of substantially less than 10‰ in every instance consistent with experiments. Thus, theory indicates that the observed $AKIE_N$s cannot be considered to rule out HAT pathways in substituted aniline oxidation for cases where active oxygen species might be generated, but neither do they need to be invoked given the good agreement between theory and electrochemical oxidation results where ET processes would be likely to be the only ones active. We note that neither the computational predictions for outer-sphere ET nor those for HAT show substituent effects consistent with those observed experimentally. This must be assigned to the simplifications inherent in the computational models, which make it challenging to reproduce the small substituent effects.

Table 1: Bulk N isotope enrichment factors, ε_N, Apparent ^{15}N-Kinetic Isotope Effects, AKIE$_N$, of Substituted Anilines in Various Experimental Systems.

Entry	Compound	pH (–)	E_h (V vs. SHE)	Conversion [a] (%)	ε_N [b] (‰)	AKIE$_N$ [b] (–)
MnO_2-suspensions						
1	Aniline [c]	7.0		55	3.6 ± 0.6	0.9960 ± 0.0009
2	*o*-CH_3-Aniline	7.0		65	6.0 ± 0.4	0.9948 ± 0.0009
3	*m*-CH_3-Aniline	7.0		53	3.7 ± 0.9	0.9963 ± 0.0006
4	*p*-CH_3-Aniline	7.0		63	6.0 ± 0.2	0.9941 ± 0.0003
5	*o*-OCH_3-Aniline	7.0		65	7.6 ± 0.2	0.9925 ± 0.0004
6	*m*-OCH_3-Aniline	7.0		52	4.9 ± 0.2	0.9952 ± 0.0001
7	*p*-OCH_3-Aniline	7.0		54	8.3 ± 0.6	0.9927 ± 0.0012
8	*p*-Cl-Aniline	7.0		88	1.3 ± 0.2	0.9987 ± 0.0004
9	*p*-CH_3-Aniline	6.0		91	5.4 ± 1.1	0.9946 ± 0.0011
10	*p*-CH_3-Aniline	5.1		35	1.1 ± 0.4	0.9986 ± 0.0007
11	*p*-CH_3-Aniline	4.7		71	-4.3 ± 2.0	1.0043 ± 0.0020
12	*p*-CH_3-Aniline	4.0		53	-6.6 ± 0.7	1.0064 ± 0.0015
13	*p*-OCH_3-Aniline	4.0		45	-5.3 ± 0.9	1.0052 ± 0.0015
14	*p*-Cl-Aniline	4.0		75	-1.9 ± 0.3	1.0019 ± 0.0006
ABTS in homogeneous solution						
15	Aniline	7.0		75	2.3 ± 0.8	0.9977 ± 0.0021
16	*p*-CH_3-Aniline	7.0		80	3.8 ± 0.1	0.9962 ± 0.0003
17	Aniline	4.0		74	-1.0 ± 0.2	1.0010 ± 0.0006
18	*p*-CH_3-Aniline	4.0		78	-4.5 ± 0.5	1.0045 ± 0.0014
Electrochemical oxidation						
19	*p*-CH_3-Aniline	7.0	0.777	56	5.2 ± 0.5	0.9948 ± 0.0013
20	*p*-CH_3-Aniline	7.0	0.837	58	6.2 ± 0.4	0.9938 ± 0.0012
21	*p*-CH_3-Aniline	7.0	0.897	50	5.6 ± 0.7	0.9944 ± 0.0017
22	*p*-CH_3-Aniline	7.0	0.957	52	3.7 ± 0.5	0.9963 ± 0.0013
23	*p*-CH_3-Aniline	4.0	0.897	73	-2.2 ± 0.3	1.0022 ± 0.0008
24	*p*-CH_3-Aniline	4.0	0.957	71	-2.5 ± 0.7	1.0025 ± 0.0019

[a] Decrease of reactant concentration / initial concentration × 100;

[b] Uncertainties correspond to 95%-confidence intervals;

[c] ε_N- and AKIE$_N$-values (Figure 1c) were derived using the Pitman estimator for combined data sets.

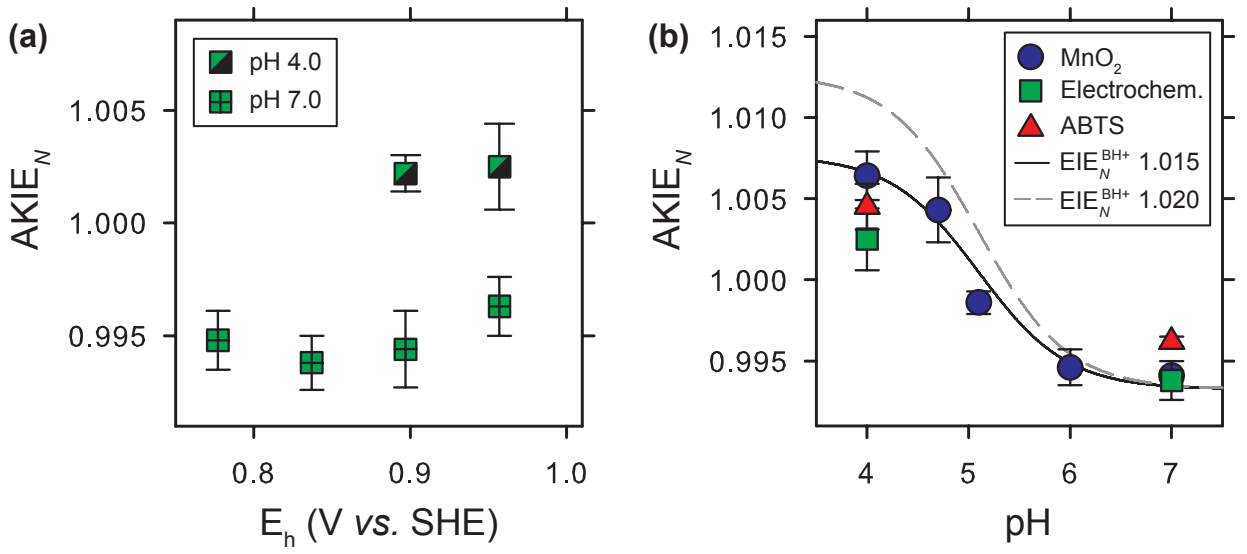

Figure 2: (a) Observed AKIE$_N$ associated with the electrochemical oxidation of *p*-CH$_3$-aniline at working electrode potential, E$_h$, between 0.78 and 0.96 V at pH 4.0 and 7.0 (see Table 1 for details); (b) Observed AKIE$_N$ of *p*-CH$_3$-aniline (pK$_{HB^+}$ 5.10) for oxidation by MnO$_2$, ABTS$^{\bullet-}$ (2,2'-azino-bis(3-ethylbenzthiazoline-6-sulfonic acid), and at a glassy carbon electrode in the pH-range 4.0 to 7.0.

Influence of substituted aniline speciation on AKIE$_N$

Because the deprotonation of substituted anilines is associated with a normal ^{15}N-equilibrium isotope effect, EIE$_N$, between 1.017 and 1.021 (*23*), we investigated the consequences of N-atom protonation on the observable N isotope fractionation trends during oxidation with selected *para*-substituted anilines in the pH-range 4.0–7.0. As shown in Table 1 (entries 4, 9-12) for *p*-CH$_3$-aniline, the AKIE$_N$ increased to almost unity at pH-values matching the pK$_{BH^+}$ and isotope fractionation became normal once the protonated species (BH$^+$) prevailed. Our data imply that ^{14}N-isotopologues reacted faster at pH < pK$_{BH^+}$ while they are outcompeted by ^{15}N-isotopologues at higher solution pH. The same trend was found for *p*-OCH$_3$-aniline (entries 7 and 13) and *p*-Cl-aniline (entries 8 and 14). Assuming that N atom oxidation can only occur from the neutral species, we propose that pH-dependent N isotope fractionation is due to a combined *normal* ^{15}N-equilibrium isotope effects pertinent to the deprotonation of the substituted anilinium cation (BH$^+$, Eq. (2)) and the *inverse* apparent ^{15}N-kinetic isotope effect associated with the oxidation of the neutral species (B, Eq. (3)) as described in Eq. (6).

Fitting the data for *p*-CH_3-aniline in Table 1 to Eq. (6) adequately describes the trends of observable $AKIE_N$ at different pH-values of the MnO_2-suspensions (Figure 2b). The calculated $AKIE_N^B$ of 0.9933 agrees well with the observed $AKIE_N$ measured at pH 7.0 (entry 4, Table 1). Deviations at pH-values below the pK_{BH^+} imply that the $EIE_N^{BH^+}$ is smaller (1.015) than proposed previously but still within the experimental uncertainty of the $EIE_N^{BH^+}$ derived for *p*-CH_3-aniline (1.0199±0.0040 (*23*)) supporting agreement of Eq. (6) with experimental data. Our interpretation of the pH-dependent, observable $AKIE_N$ is supported by the results from reference experiments regarding the electrochemical and homogeneous oxidation of aniline and *p*-CH_3-aniline at pH 4.0 and 7.0. The trends of $AKIE_N$ *vs.* pH for oxidation at glassy carbon electrode surfaces and by $ABTS^{\bullet-}$ were very similar to the ones observed in MnO_2-suspensions (Figure 2b, Table 1). These results confirm that at pH-values below the pK_{BH^+}, N isotope fractionation approaches the product of equilibrium and kinetic ^{15}N-isotope effects (Eq. (6)), where the measured $AKIE_N$ values are dominated by the normal EIE. As a final check, we evaluated the predicted KIEs for HAT from protonated anilines by active oxygen species $^{\bullet}OH$ / $^{\bullet}OOH$ (Table S1, entries 38-43). In all cases, N isotope effects were predicted to be inverse (Table S1), providing further evidence that the observed normal N isotope effects reflect acid/base partitioning prior to oxidation of the conjugate base.

Environmental Significance

Our study illustrates that oxidation of primary aromatic amino groups in organic contaminants is accompanied by a small and measurable N isotope fractionation thus enabling new avenues for the assessment of degradation reactions at N-containing functional groups. Because the pK_{BH^+} of many aromatic amines are in the range of pH-values encountered in many aquatic systems, the observable N isotope fractionation will be modulated substantially by the compound's acid/base equilibria. Isotope fractionation may even vanish under conditions where contributions from *normal* EIE_N associated with aromatic deprotonation and *inverse* $AKIE_N$ of N atom oxidation cancel each other out. This variability of N isotope fractionation slightly complicates the application of CSIA in that the contaminant's pK_{BH^+} and solution pH have to be taken into account. The system-

atic trends of $AKIE_N$-values, on the other hand, provide a new line of evidence for the identification of contaminant degradation processes via reactions of primary aromatic amino groups.

Nitrogen isotope enrichment factors below 10‰ at the reactive position, as reported in this study, imply that δ^{15}N-measurements should be carried out with small total uncertainties ($<\pm 0.5$‰) and require that N isotope fractionation is not diluted by many non-reactive N atoms in a contaminant. The impact of substituent properties on $AKIE_N$-values suggest that contaminant-specific ε_N-values will be required to assess their oxidation processes by CSIA. The compound-specific N isotope fractionation behavior contrasts earlier observations for the reduction of aromatic nitro groups (*14*, *42*), which found $AKIE_N$-values that were largely independent of the compound's molecular structure. The substituent-dependence might, together with the influence of acid/base equilibria, prove indicative for the identification of N aryl oxidation processes. Further studies targeting N isotope fractionation in alternative contaminant transformation processes such as oxidative N-dealkylations and nucleophilic additions are warranted to evaluate the proposed trends of N isotope effects.

Acknowledgement

This work was supported by the Swiss National Science Foundation (grant no. 200020-116447/1 to T.B.H.) and the U.S. National Science Foundation (CHE-0952054 to. C.J.C). We thank Jakov Bolotin for experimental support, Michael Aeschbacher and Michael Sander for supporting the electrochemical experiments, Michael Plötze for assisting the BET- and XRD-measurements, Brian Sinnet for his help with ζ-potential measurements, Susanne Kern and Heinz Singer for assisting the LC-MS/MS-measurements and Maarten Nachtegaal and Markus Janousch for conducting the XANES-measurements. We acknowledge XD10A SuperXAS beamline of the SLS-PSI for the provision of beam time.

Supporting Information Available

Chemicals used, preparation and characterization of MnO_2-suspension (includes XRD, XANES, specific surface area and pH_{IEP} measurements), kinetics of aniline oxidation in MnO_2-suspensions, mathematical derivation of $AKIE_N^{BH^+}$, DFT calculations of ET- and HAT-KIE_N, compilation of detected oxidation products, C isotope fractionation. This material is available free of charge via the Internet at http://pubs.acs.org/.

References

(1) Klausen, J.; Haderlein, S. B.; Schwarzenbach, R. P. Oxidation of substituted anilines by aqueous MnO_2: Effect of co-solutes on initial and quasi steady state kinetics. *Environ. Sci. Technol.* **1997**, *31*, 2642–2649.

(2) Laha, S.; Luthy, R. G. Oxidation of aniline and other primary aromatic amines by manganese dioxide. *Environ. Sci. Technol.* **1990**, *24*, 363–373.

(3) Zhang, H. C.; Huang, C. H. Oxidative transformation of fluoroquinolone antibacterial agents and structurally related amines by manganese oxide. *Environ. Sci. Technol.* **2005**, *39*, 4474–4483.

(4) Bialk, H. M.; Pedersen, J. A. NMR investigation of enzymatic coupling of sulfonamide antimicrobials with humic substances. *Environ. Sci. Technol.* **2008**, *42*, 106–112.

(5) Dodd, M.; Buffle, M.; Gunten, U. V. Oxidation of antibacterial molecules by aqueous ozone: Moiety-specific reaction kinetics and application to ozone-based wastewater treatment. *Environ. Sci. Technol.* **2006**, *40*, 1969–1977.

(6) Paul, T.; Dodd, M. C.; Strathmann, T. J. Photolytic and photocatalytic decomposition of aqueous ciprofloxacin: Transformation products and residual antibacterial activity. *Water Res.* **2010**, *44*, 3121–3132.

(7) Schwarzenbach, R. P.; Egli, T.; Hofstetter, T. B.; von Gunten, U.; Wehrli, B. Global water pollution and human health. *Annu. Rev. Environ. Resour.* **2010**, *35*, 109–136.

(8) Shin, K. A.; Spain, J. C. Pathway and evolutionary implications of diphenylamine biodegradation by *Burkholderia* sp. Strain JS667. *Appl. Environ. Microbiol.* **2009**, *75*, 2694–2704.

(9) Thorn, K. A.; Pettigrew, P. J.; Goldenberg, W. S.; Weber, E. J. Covalent binding of aniline to humic substances. 2. ^{15}N-NMR studies of nucleophilic addition reactions. *Environ. Sci. Technol.* **1996**, *30*, 2764–2775.

(10) Elsner, M. Stable isotope fractionation to investigate natural transformation mechanisms of organic contaminants: principles, prospects and limitations. *J. Environ. Monit.* **2010**, *12*, 2005–2031.

(11) Hofstetter, T. B.; Berg, M. Assessing transformation processes of organic contaminants by compound-specific stable isotope analyses. *TrAC-Trends Anal. Chem.* **2011**, *30*, 618–627.

(12) Hofstetter, T. B.; Schwarzenbach, R. P.; Bernasconi, S. M. Assessing transformation processes of organic compounds using stable isotope fractionation. *Environ. Sci. Technol.* **2008**, *42*, 7737–7743.

(13) Wolfsberg, M.; van Hook, A.; Paneth, P.; Rebelo, L. P. N. *Isotope Effects in Chemical, Geological, and Bio Sciences*; Springer: Heidelberg, 2010.

(14) Hartenbach, A.; Hofstetter, T. B.; Aeschbacher, M.; Sander, M.; Kim, D.; Strathmann, T. J.; Arnold, W. A.; Cramer, C. J.; Schwarzenbach, R. P. Variability of nitrogen isotope fractionation during the reduction of nitroaromatic compounds with dissolved reductants. *Environ. Sci. Technol.* **2008**, *42*, 8352–8359.

(15) Hartenbach, A.; Hofstetter, T. B.; Berg, M.; Bolotin, J.; Schwarzenbach, R. P. Using nitrogen isotope fractionation to assess abiotic reduction of nitroaromatic compounds. *Environ. Sci. Technol.* **2006**, *40*, 7710–7716.

(16) Hofstetter, T. B.; Spain, J. C.; Nishino, S. F.; Bolotin, J.; Schwarzenbach, R. P. Identifying competing aerobic nitrobenzene biodegradation pathways using compound-specific isotope analysis. *Environ. Sci. Technol.* **2008**, *42*, 4764–4770.

(17) Penning, H.; Cramer, C. J.; Elsner, M. Rate-dependent carbon and nitrogen kinetic isotope fractionation in hydrolysis of isoproturon. *Environ. Sci. Technol.* **2008**, *42*, 7764–7771.

(18) Penning, H.; Sorensen, S. R.; Meyer, A. H.; Aamand, J.; Elsner, M. C, N, and H isotope fractionation of the herbicide isoproturon reflects different microbial transformation pathways. *Environ. Sci. Technol.* **2010**, *44*, 2372–2378.

(19) Hartenbach, A. E.; Hofstetter, T. B.; Tentscher, P. R.; Canonica, S.; Berg, M.; Schwarzenbach, R. P. Carbon, hydrogen, and nitrogen isotope fractionation during light-induced transformations of atrazine. *Environ. Sci. Technol.* **2008**, *42*, 7751–7756.

(20) Meyer, A. H.; Penning, H.; Elsner, M. C and N isotope fractionation suggests similar mechanisms of microbial atrazine transformation despite involvement of different enzymes (AtzA and TrzN). *Environ. Sci. Technol.* **2009**, *43*, 8079–8085.

(21) Dybala-Defratyka, A.; Szatkowski, L.; Kaminski, R.; Wujec, M.; Siwek, A.; Paneth, P. Kinetic isotope effects on dehalogenations at an aromatic carbon. *Environ. Sci. Technol.* **2008**, *42*, 7744–7750.

(22) Gorski, C. A.; Nurmi, J. T.; Tratnyek, P. G.; Hofstetter, T. B.; Scherer, M. M. Redox behavior of magnetite: Implications for contaminant reduction. *Environ. Sci. Technol.* **2010**, *44*, 55–60.

(23) Skarpeli-Liati, M.; Arnold, W. A.; Turgeon, A.; Cramer, C. J.; Hofstetter, T. B. pH-dependent equilibrium isotope fractionation associated with compound-specific nitrogen and carbon isotope analysis by SPME-GC/IRMS. *Anal. Chem.* **2011**, *83*, 1641–1648.

(24) Murray, J. W. Surface Chemistry of Hydrous Manganese-Dioxide. *J. Colloid Interface Sci.* **1974**, *46*, 357–371.

(25) Kern, S.; Fenner, K.; Singer, H. P.; Schwarzenbach, R. P.; Hollender, J. Identification of transformation products of organic contaminants in natural waters by computer-aided prediction and high-resolution mass spectrometry. *Environ. Sci. Technol.* **2009**, *43*, 7039–7046.

(26) Aeschbacher, M.; Sander, M.; Schwarzenbach, R. P. Novel electrochemical approach to assess the redox properties of humic substances. *Environ. Sci. Technol.* **2010**, *44*, 87–93.

(27) Lollar, B. S.; Hirschorn, S. K.; Chartrand, M. M. G.; Lacrampe-Couloume, G. An approach for assessing total instrumental uncertainty in compound-specific carbon isotope analysis: Implications for environmental remediation studies. *Anal. Chem.* **2007**, *79*, 3469–3475.

(28) Scott, K. M.; Lu, X.; Cavanaugh, C. M.; Liu, J. S. Optimal methods for estimating kinetic isotope effects from different forms of the Rayleigh distillation equation. *Geochim. Cosmochim. Acta* **2004**, *68*, 433–442.

(29) Tobler, N. B.; Hofstetter, T. B.; Schwarzenbach, R. P. Carbon and hydrogen isotope gractionation during anaerobic toluene oxidation by *Geobacter metallireducens* with different Fe(III) phases as terminal electron acceptors. *Environ. Sci. Technol.* **2008**, *42*, 7786–7792.

(30) Perdew, J.; Yue, W. Accurate and simple density functional for the electronic exchange energy: Generalized gradient approximation. *Phys. Rev. B* **1986**, *33*, 8800–8802.

(31) Perdew, J. P. In *Unified Theory of Exchange and Correlation Beyond the Local Density Approximation*; Ziesche, E. H., P., Ed.; Electronic Structure of Solids; Akademie Verlag, Berlin: p. 11-20, 1991.

(32) Adamo, C.; Barone, V. Exchange functionals with improved long-range behavior and adiabatic connection methods without adjustable parameters: The mPW and mPW1PW models. *J. Chem. Phys.* **1998**, *108*, 664–675.

(33) Hehre W., S. P., Radom L. *Ab Initio Molecular Orbital Theory*; Wiley: New York, 1986.

(34) Cramer, C. J. *Essentials of Computational Chemistry: Theories and Models*, 2nd ed.; John Wiley & Sons: Chichester, 2004.

(35) Kavner, A.; Bonet, F.; Shahar, A.; Simon, J.; Young, E. The isotopic effects of electron transfer: An explanation for Fe isotope fractionation in nature. *Geochim. Cosmochim. Acta* **2005**, *69*, 2971–2979.

(36) Zhang, H. C.; Chen, W. R.; Huang, C. H. Kinetic modeling of oxidation of antibacterial agents by manganese oxide. *Environ. Sci. Technol.* **2008**, *42*, 5548–5554.

(37) Zhu, M. Q.; Paul, K. W.; Kubicki, J. D.; Sparks, D. L. Quantum chemical study of arsenic (III/V) adsorption on Mn-oxides: Implications for arsenic(III) oxidation. *Environ. Sci. Technol.* **2009**, *43*, 6655–6661.

(38) Nesbitt, H. W.; Canning, G. W.; Bancroft, G. M. XPS study of reductive dissolution of 7 Å-birnessite by H_3AsO_3, with constraints on reaction mechanism. *Geochim. Cosmochim. Acta* **1998**, *62*, 2097–2110.

(39) Pretsch E., A. C., Bühlmann P.; M., B. *Spektroskopische Daten zur Strukturaufklärung organischer Verbindungen*, 4th ed.; Springer Verlag, 2001.

(40) Fitzpatrick, P. F. Oxidation of amines by flavoproteins. *Arch. Biochem. Biophys.* **2010**, *493*, 13–25.

(41) Ralph, E. C.; Hirschi, J. S.; Anderson, M. A.; Cleland, W. W.; Singleton, D. A.; Fitzpatrick, P. F. Insights into the mechanism of flavoprotein-catalyzed amine oxidation from nitrogen isotope effects on the reaction of N-methyltryptophan oxidase. *Biochemistry* **2007**, *46*, 7655–7664.

(42) Hofstetter, T. B.; Neumann, A.; Arnold, W. A.; Hartenbach, A. E.; Bolotin, J.; Cramer, C. J.; Schwarzenbach, R. P. Substituent effects on nitrogen isotope fractionation during abiotic reduction of nitroaromatic compounds. *Environ. Sci. Technol.* **2008**, *42*, 1997–2003.

TOC graph